M&C 2001 Salt Lake City, Utah, USA, September 2001.

ADJOINT CHARGE DEPOSITION AND CAD TRANSPORT IN ITS

Brian C. Franke, Ronald P. Kensek, Heather K. Schriner,
Leonard J. Lorence, and Fred Gelbard
Sandia National Laboratories
Albuquerque, NM 87185-1179
bcfrank@sandia.gov rpkense@sandia.gov

Steve Warren
Kansas State University

Keywords: adjoint charge deposition, CAD, Monte Carlo, Integrated TIGER Series, ITS

ABSTRACT

We present an adjoint method for calculating charge deposition that has been implemented in the ITS Monte Carlo codes and discuss the extension of the ITS codes to CAD geometries. Using multigroup coupled-electron-photon cross sections in a version of the Monte Carlo code ITS, we demonstrate the effectiveness of the adjoint charge-deposition method by comparing numerical results with experimental benchmarks. The strengths and weaknesses of this method relative to forward calculations are examined. The methods involved in the development of a CAD-geometry capability for ITS are also presented. Using the physics of the ITS codes to perform radiation transport in CAD geometries is more computationally expensive, but may decrease the time involved in problem setup and later geometry modification. Possible applications for these new methods are discussed.

1. INTRODUCTION

Charge-deposition calculations are generally quite difficult to perform using the Monte Carlo method. The net charge deposited is the difference of two quantities, charge removed due to interactions imparting energy to secondary charged particles and charge deposited due to the "absorption" of charged particles slowing down in the medium. Obtaining a good statistical estimate of the net charge deposited can be difficult when the result is near zero.

In a forward calculation, one specifies a forward source and may examine numerous detector responses in a single calculation. In an adjoint calculation, one specifies the type and region of the detector response of interest and may examine the response due to numerous forward sources in a single calculation. For photon sources, electronic equilibrium may exist throughout most of the problem, and charge deposition may be a highly localized phenomenon near material interfaces. The adjoint mode allows us to examine the detector response near material interfaces and focus the problem on the localized charge deposition.

Morel, et al. (1996), described the algorithm implemented in the multigroup ITS Monte Carlo coupled electron-photon code and demonstrated the accuracy of the adjoint method for energy-deposition calculations. Lorence, et al. (1995), presented results from the multigroup ITS (MITS) code demonstrating the effectiveness of the adjoint method for the energy-deposition and particle-escape detector responses. The contribution of this work is the extension of the adjoint capability in MITS to charge deposition.

One of the difficulties of performing transport calculations on complex geometries is the time required to construct a model of the geometry. In many cases, a model of the geometry may already exist in another format, such as CAD. In this paper we describe some of the methods used to interface the physics of ITS with a commercial CAD program. While this approach is computationally expensive, it can eliminate the time required to construct a combinatorial-geometry model.

In Section 2 of this paper, we present the unique transport mechanisms required for the adjoint charge-deposition method. In Section 3, we discuss some special considerations involved in performing adjoint charge-deposition calculations. In Section 4, we present comparisons of charge-deposition calculations with experimental data, and we discuss calculations performed with a complex geometry model of a satellite. In Section 5, we describe the new CAD-geometry capability in the ITS codes. In Section 6, we offer some conclusions on these methods.

2. ADJOINT PARTICLE SOURCE FOR CHARGE DEPOSITION

The hybrid multigroup/continuous-energy electron-photon Monte Carlo method implemented in the MITS code has been described in detail by Morel, et al. (1996). In this approach, both Boltzmann and Fokker-Planck interactions are represented. Multigroup cross section data are obtained from the CEPXS code (Lorence, 1989). The theory of adjoint charge deposition, while not presented in the previous work, can be derived from it. To implement an adjoint charge-deposition capability, it was necessary to develop the proper source of adjoint particles and make slight modifications to the form of the low-energy cross sections used. Those developments are described in this section.

Charge deposition is the result of the difference between the removal and absorption of charged particles in a medium. Removal is due to particle interactions imparting energy to electrons (or positrons) sufficient to transport the secondary particles to another region of material. In radiation transport codes, this is the production of secondary charged particles above the cutoff energy due to Boltzmann interactions. Absorption results from charged-particle interactions that leave the particle with less than the cutoff energy. In the MITS implementation, a charged particle may fall below the cutoff energy due to either the continuous-slowing-down (CSD) operator or an inelastic Boltzmann interaction.

For adjoint calculations, it is necessary to formulate a source of adjoint particles based on the reaction cross sections. The ITS codes calculate “charge” deposition in units of number of electrons deposited. Thus, in our implementation adjoint particles corresponding to secondary-electron-production interactions are initiated with a negative

weight, and those corresponding to electron absorption are initiated with a positive weight. The charge-deposition cross sections due to Boltzmann interactions are discussed in Section 2.1. The charge-deposition cross section from charged particles falling below the cutoff energy due to the CSD operator is discussed in Section 2.2.

2.1 Boltzmann-Interaction Contributions to Charge Deposition

For most multigroup calculations, charged particles in the lowest-energy group are of the least importance, especially when the typical logarithmic energy-group structure is employed. These particles have little energy to deposit and are unlikely to produce secondary radiation. Even in a forward charge-deposition calculation where the weight of the particle in the tally makes it as important as any other, the relatively short range may make the transport of the particle unimportant. However, in an adjoint charge-deposition calculation a significant fraction of all adjoint particles, and most of the particles contributing positively to the electron deposition, will pass through the lowest-energy electron group. The accurate modeling of the physics in this lowest-energy group is very important to an accurate calculation.

To perform the adjoint inversion of the multigroup cross sections in MITS, each group must have an inelastic Boltzmann-interaction component. A finite total cross section is necessary for the possibility of any inelastic Boltzmann interactions in a group. A finite total cross section is also necessary to determine the number of higher-energy adjoint particles produced per interaction from the lowest-energy group,

$$N_g = \Sigma_{g \to L} \cdot \frac{\Delta E_g}{\Delta E_L} \cdot \frac{1}{\Sigma_{tL}}. \tag{1}$$

N_g is the number of particles produced in group g per inelastic Boltzmann interaction in group L; $\Sigma_{g \to L}$ is the forward scattering cross section from group g to group L; the ratio of the width of energy group g, ΔE_g, to the width of energy group L, ΔE_L, is the adjoint inversion of the scattering cross section; and Σ_{tL} is the total inelastic Boltzmann-interaction cross section in the lowest-energy group. This total cross section in the MITS implementation does not include Fokker-Planck or elastic interactions, but it does include absorption interactions. Note that as the total cross section goes to zero, the probability of an interaction will go to zero while the number of adjoint particles produced per interaction will go to infinity.

For the lowest-energy group, we must introduce some form of Boltzmann interaction. We can do this by including an effective-absorption cross section based on elastic scattering to a pseudo-group below the cutoff energy. For the forward calculation, the magnitude of the effective-absorption cross section is arbitrary as long as the rate of energy loss is preserved. However, we can base this absorption on a physical process.

To maintain energy-loss straggling in MITS, it was found necessary to include a Boltzmann operator for scattering between adjoining groups based on an approximation to the transfer of particles between adjoining groups (Morel, 1996). The stopping power associated with transfers between adjacent groups is

$$S_{g\to g+1} = \frac{\int_{E_{g+1}}^{E_g} dE \int_{E_{g+2}}^{E_{g+1}} dE'(E-E')\Sigma(E\to E')}{E_g - E_{g+1}}. \quad (2)$$

Here, E_g is the upper energy bound of group g, E_{g+1} is the lower energy bound of group g, E_{g+2} is the lower energy bound of group g+1, and $\Sigma(E\to E')$ is the scattering cross section from energy E to energy E'. Because the integral in Eq. (2) is singular in the CEPXS implementation (Lorence, 1989), Eq. (2) is replaced by

$$\beta_{g\to g+1} = \Sigma(E_g^m \to E_{g+1}^m)\times(E_g^m - E_{g+1}^m)\times(E_{g+1} - E_{g+2}). \quad (3)$$

Here, E_g^m is the mid-point energy of group g. The Boltzmann-scattering cross section from group g to group g+1 is then calculated as

$$\Sigma_{g\to g+1} = \frac{\beta_{g\to g+1}}{E_g^m - E_{g+1}^m}. \quad (4)$$

We can use the same scattering process between the lowest-energy group and a pseudo-group below the cutoff energy as the basis for an effective-absorption cross section in the lowest-energy group,

$$\Sigma_{aL} = \frac{\beta_{L\to L+1}}{E_L^m - E_{L+1}^m}. \quad (5)$$

Σ_{aL} is the absorption cross section in the lowest-energy electron group, L is the lowest-energy group that is included in the transport calculation, and L+1 is the pseudo-group below the cutoff energy. The presence of this inelastic Boltzmann interaction allows the cross sections for scattering from a higher-energy group to the lowest-energy group to be inverted using Eq. (1) within the MITS formulation.

We would like to impose two constraints on this technique. The first is preservation of the rate of energy loss within the lowest-energy group. Within CEPXS, the restricted stopping power for the last group is calculated as the true stopping power minus the approximate value for transfers between adjacent groups, $\beta_{g\to g+1}$. Therefore, the rate of energy loss within the group is preserved. The second constraint is that the particle flux remains approximately constant as a function of energy in the lowest-energy group. This is the basis of the multigroup approximation. If the effective-absorption cross section in the lowest-energy group is too large, then the particle flux will not be constant across the group. This requirement of a "small" effective-absorption cross section can be expressed as

$$1 \approx \exp\left(-\Sigma_{aL}\frac{\Delta E_L}{S_L}\right), \quad (6)$$

where S_L is the restricted stopping power in the lowest-energy group.

It should be noted that we have not yet defined the mid-point energy of the pseudo-group used in Eq. (5). In the following section, we will do so on the assumption that the condition of a small effective-absorption cross section is met.

2.1.2 Cutoff Contributions to Charge Deposition

In the forward mode, particles reaching the cutoff energy via CSD are absorbed with dose and charge deposited locally. Therefore, when adjoint dose or charge calculations are performed, it is necessary to initiate the proper number of adjoint particles at the cutoff energy based upon this absorption rate. Morel, et al. (1996), showed that the rate of electron absorption at the cutoff energy is the stopping power at the cutoff times the electron flux at the cutoff. Therefore, the weight of adjoint electrons initiated at the cutoff energy for charge deposition should be

$$W_c = S_c , \tag{7}$$

where S_c is the stopping power at the cutoff energy.

In the adjoint formulation, when a charged particle speeds up from one group to the next, the weight is adjusted by the ratio of the stopping powers (Halbleib, 1980), or analogously, the particle is subjected to Russian Roulette with a survival probability proportional to the ratio of the stopping powers. When an adjoint electron is created at the cutoff energy, it immediately speeds up into the lowest-energy group. Even if we produce particles using Eq. (7) with the exact stopping power at the cutoff, we must immediately adjust their weights by the ratio of the stopping power in the lowest energy group to the stopping power at the cutoff energy. If we use Russian Roulette, the effect is the same as if we produce particles at the cutoff energy using the stopping power of the lowest-energy group. Therefore, for implementation purposes, we replace Eq. (7) with

$$W_c = S_L . \tag{8}$$

If the effective-absorption cross section in the lowest-energy group is small, then relatively few adjoint particles will suffer Boltzmann collisions in the lowest-energy group. This being the case, we can make the requirement of conservation of the number of adjoint particles started at the cutoff and in the lowest-energy group a condition for determining the size of the pseudo-group upon which the effective-absorption cross section is based.

The weight of adjoint particles initiated in group g is

$$W_g = \Sigma_{dep} \Delta E_g , \tag{9}$$

where Σ_{dep} is the charge-deposition cross section. In the lowest-energy group, charge deposition is only due to absorption. Therefore, for the lowest-energy group Eq. (9) may be written as

$$W_L = \Sigma_{aL} \Delta E_L \,. \tag{10}$$

The effective-absorption in the lowest-energy group is given by Eq. (5). When we include the effective-absorption cross section and modify the stopping power in lowest-energy group to a restricted stopping power by subtracting $\beta_{L \to L+1}$, we would like to preserve the weight of adjoint particles produced in Eq. (8). Therefore, we arrive at the requirement that

$$E_{L+1}^m = E_L^m - \Delta E_L \,. \tag{11}$$

This means that the energy width of the pseudo-group must be equal to the energy width of the lowest-energy group. With a pseudo-group of this size, the condition of a small effective-absorption cross section appears to be met for most reasonable energy-group structures.

3. CHARGE-DEPOSITION CONSIDERATIONS

An important consideration in adjoint charge-deposition calculations is the choice of the cutoff energy in the generation of cross sections. A high cutoff energy may result in inaccuracies near material interfaces, as in a forward calculation. A low cutoff energy will result in a less-efficient adjoint calculation. A low cutoff energy yields larger secondary-production cross sections at high energies and larger absorption cross sections at low energies. Therefore, away from material interfaces, more time is spent on the transport of particles that represent offsetting contributions to charge deposition. The development of adjoint sources that employ charge-deposition cross sections with a geometry-dependent cutoff energy is being investigated. This is analogous to electron trapping in forward calculations and may alleviate the considerations involved in choosing a proper cutoff energy.

While not explicitly discussed in the preceding section, similar considerations apply to the simulation of positrons in adjoint charge-deposition calculations. The capability to simulate positrons in adjoint mode and the adjoint equivalent of the annihilation process have been implemented in MITS. However, in most calculations of energy or charge deposition an approximation can be made to avoid the simulation of positrons. The same approximations employed in forward calculations can be used for adjoint calculations. For charge-deposition calculations, pair production can be replaced by the production of two annihilation photons at the site of pair production. This approximation generally has little effect on the speed of forward Monte Carlo calculations, but it can significantly affect the efficiency of adjoint Monte Carlo charge-deposition calculations.

4. NUMERICAL RESULTS

In this section, we present results for three different types of adjoint charge-deposition calculations. First, one-dimensional calculations for a volume detector response are compared with forward calculations and experimental data. Second, one-dimensional calculations with point detector responses are compared with a forward

calculation and a similar forward calculation is compared with experimental measurements of charge deposition as a function of depth from an electron source. Third, point charge-deposition calculations are presented in a silicon chip inside of a three-dimensional satellite model. We acknowledge that the first two examples are more efficiently solved with forward Monte Carlo calculations and are presented for validation purposes. The third example is more representative of an effective use of the adjoint charge-deposition capability.

4.1 Lockwood Data

Lockwood, et al. (1980), measured total charge deposition from mono-directional electron beams incident on material slabs. For each material, multiple electron energies and angles of incidence were examined. A volumetric adjoint charge-deposition calculation in a slab can be directly compared with this data. Furthermore, this problem illustrates one of the potential strengths of an adjoint calculation, that a single detector response can be analyzed for numerous forward sources in a single calculation. Lorence, et al. (1995), presented a similar comparison between the MITS code and the Lockwood data. However, that comparison was based on an adjoint electron-escape response that in this problem is the complement of the charge-deposition response.

The results of a MITS adjoint calculation, MITS forward calculations, and the Lockwood data for electron beams incident on a uranium slab are shown in Fig. 1. All MITS calculations were performed with a 10-keV cutoff energy. The adjoint results are based on forward sources in each of 50 energy groups with an angular spread of ±7.5 degrees from the experimental angle of incidence. The adjoint calculation required approximately 73 processor-days and yielded better than 1 percent statistics for most of the data shown, except for the normally-incident direction that had approximately 1-2 percent statistics. The forward calculations simulated the experimental angles of incidence and required a cumulative time of approximately 2.4 processor-hours and yielded better than 0.5 percent statistics. All computation times in this paper are given for calculations performed using 330-MHz processors on the ASCI-RED machine.

The forward and adjoint numerical results are in good agreement and provide verification that the angular bins in the adjoint calculation are sufficiently refined. (The results of forward calculations with the same forward-source angular distributions as the adjoint calculation yielded statistical agreement with the adjoint calculation to provide verification of our implementation.) In comparison with the experimental results, the MITS results appear to systematically under-estimate the charge deposition in the slab. The agreement is best at normal incidence and degrades with increasing angle of incidence. The data for 32-keV electrons at high angles of incidence shows the poorest agreement. More than half of the forward results are within 5 percent of the experimental data. Except for at the lowest energy or the highest angle of incidence, all of the forward results are within 10 percent of the experimental data. The cause of the disagreements is being investigated by comparisons for other materials and comparisons with the continuous-energy ITS code. We also note an observable transition in the MITS results near 256 keV for all angles of incidence. This artifact is due to the use of screened Mott cross sections above 256 keV and Riley cross sections below 256 keV.

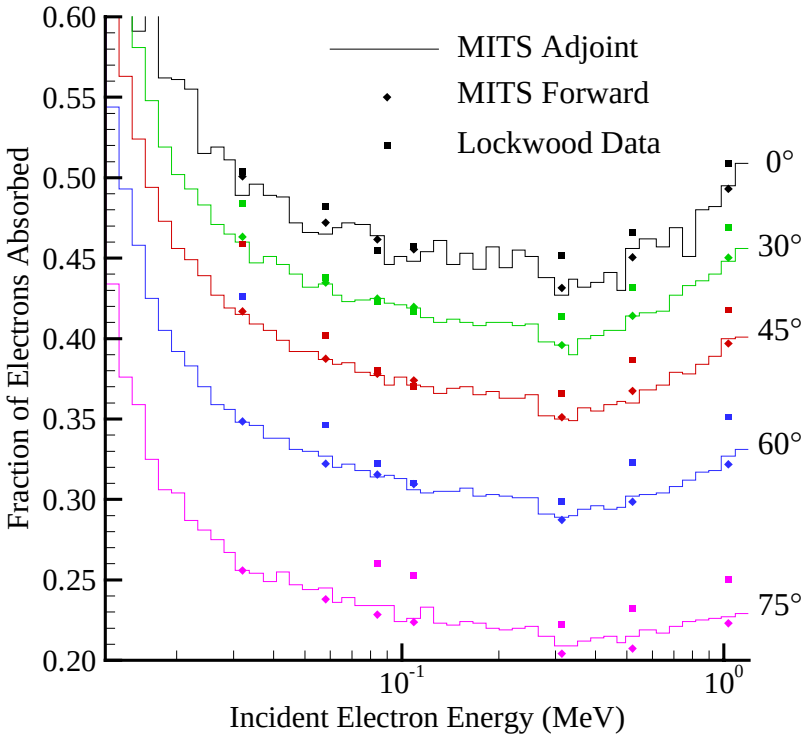

Fig. 1 Comparison of adjoint charge-deposition calculation and Lockwood data in uranium as a function of energy for varying electron-beam incidence angles.

4.2 Tabata Data

Tabata, et al. (1971), measured the distributions of charge deposition due to normally-incident mono-energetic electron beams on thick absorbers. Detector responses due to singular sources are difficult to calculate in adjoint calculations. The Lockwood data also used singular forward sources, but the total charge deposition is less sensitive than the spatial distribution of charge deposition to the energy and angular distribution of the forward source. For the Tabata data, a direct comparison of the data with adjoint calculations is not practical. However, we can compare a forward calculation to the experimental data and compare adjoint calculations to a similar forward calculation.

In Fig. 2, we show that the forward multigroup calculation yields a charge-deposition profile in excellent agreement with the experimental data for a 14.9-MeV electron source that is normally incident on a slab of aluminum. The forward calculation was performed using a normally-incident, mono-energetic electron beam with cross sections consisting of 100 logarithmic energy groups and a 10-keV cutoff energy. Charge deposition was calculated in slabs that were 0.0675-g/cm^2 thick.

In Fig. 3, we show that adjoint point-charge-deposition calculations appear to be within statistical agreement of a forward calculation with an identical source. For both the adjoint and forward calculations, the forward electron source was distributed as a cosine-law between 0 and 20 degrees to the normal. Both calculations were performed

using cross sections consisting of 25 logarithmic energy groups and a 60-keV cutoff energy. The forward sources in these Monte Carlo calculations were uniformly distributed within the highest-energy group spanning 13.31 to 16.67 MeV.

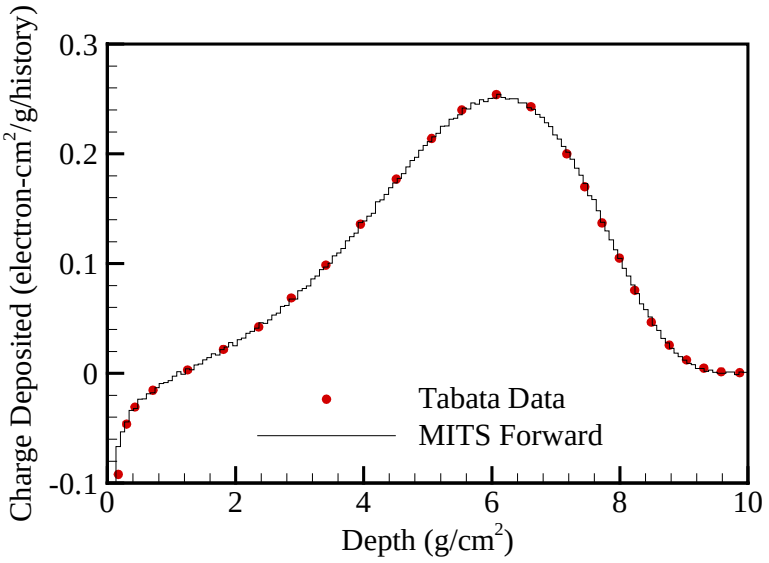

Fig. 2 Comparison of forward MITS charge-deposition calculation and Tabata data for a normally incident, 14.9-MeV electron beam on an infinite slab of aluminum.

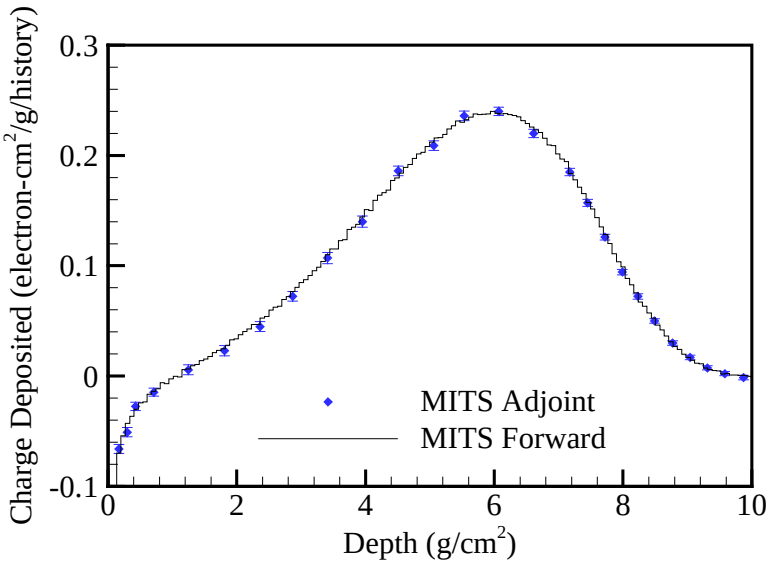

Fig. 3 Comparison of MITS charge-deposition calculations in forward and adjoint modes for a 14.9-MeV electron beam distributed as a cosine-law between 0 and 20 degrees to the normal on an infinite slab of aluminum.

4.3 Charge Deposition in STARSAT Electronics Box

Fig. 4 depicts the combinatorial-geometry (CG) model of STARSAT that is used in the 3-D charge-deposition calculations to be discussed (Varcolik, 1988). The model of this satellite is comprised of a total of more than 600 CG bodies. Portions of the satellite are approximated as reduced-density materials distributed over regions that in reality are a combination of void and intricate geometries. Within the satellite, the Attitude Control Electronics (ACE) box is more accurately modeled with more than 200 CG bodies.

Fig. 4 STARSAT combinatorial-geometry model.

Adjoint charge-deposition calculations were performed at various locations inside of the ACE box in the satellite. A forward photon source was distributed uniformly in energy between 1 and 50 keV. The unit sphere of possible source directions was divided into 472 bins of approximately equal solid angles, and all possible source directions were recorded in these bins. Each direction on the unit sphere represents an infinite-plane source incident on the satellite from that direction.

Fig. 5 shows the dependence of charge deposition on the direction of incidence of an infinite-plane photon source. Each unit sphere represents one of the four corners of a silicon chip in the ACE box on the face nearest to the outer surface of the satellite. The spheres are displayed from the direction of normal to that face of the chip. The lower right sphere is the result of a calculation requiring approximately 12 processor-days. This yielded six-percent statistics for the direction of greatest vulnerability. The other three calculations each required approximately 3.7 processor-days. These calculations yielded 10-15 percent statistics for the directions of greatest vulnerability. In the longer calculation, the better statistics are noticeable in the decreased fluctuation of data and decreased number of negative values.

The effects of two features of the geometry are discernable in this assessment of directions of vulnerability. The solar panel creates a vertical “shadow” slightly to the right of center in each plot. Another effect is due to a kovar cover on the silicon chip.

This cover is thinnest on the sides of the chip in the x-dimension. This is revealed in the "shadowing" of the right halves of the two left spheres and of the left halves of the two right spheres.

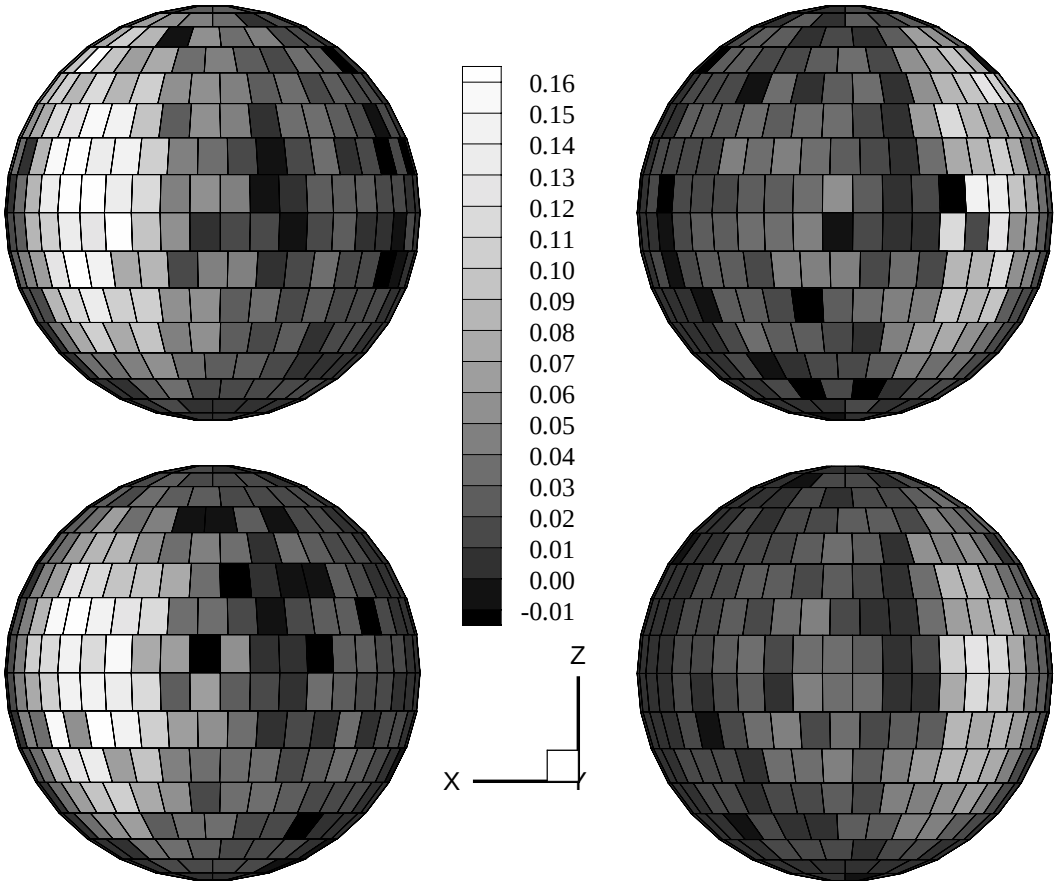

Fig. 5 The charge deposition (in units of electron-cm^2/g/photon) calculated at the corners of a silicon chip in the STARSAT ACE box. The results at each corner are shown on unit spheres as a function of exposure angle.

A forward Monte Carlo calculation of the charge deposition in the chip is much less practical than an adjoint charge-deposition calculation. This is due to the complex geometry of the satellite, the small size of the silicon chip relative to the satellite, and the overall difficulty of Monte Carlo charge-deposition calculations. A heavily-biased calculation relying on user judgements about the importance of directions of exposure and about the dominant interaction effects might make a forward calculation possible but could jeopardize the fidelity of the results.

5. ITS-CAD: Using ITS with CAD geometries

The three-dimensional geometry model of the MITS code is the same as that for the continuous-energy ITS code described by Halbleib, et al. (1992). In this "combinatorial geometry" (CG) approach, the geometry is constructed from Boolean

operations on simple geometric primitives (sphere, cylinder, etc.). This model has proven to be rather efficient from a computational run-time perspective, but can require enormous investments in both problem setup and later modification.

Presently, it is not uncommon for objects requiring radiation transport analysis to have been designed by CAD software – i.e., a mathematical model already exists, but one that is not compatible with the existing code. We have implemented a scheme to make use of these CAD models more directly. These modifications are described in this section.

We decided to use commercial library routines based on the ACIS™ file format (Spatial Technology, 2000), based on the following reasons:

- Use of the most recent library routines will automatically be up to date as opposed to trying to write and maintain our own routines.
- ACIS™ is already in use at our laboratory and we have a site license for source code. Further, it is a format common to several commercial CAD packages so translation from another format into ACIS™ may be possible if necessary.
- Direct use of the CAD model will provide a more accurate description of material boundaries. It also uses less memory than a derived finite-element mesh, especially for adjoint calculations where spatial profiles are not calculated.
- General translation from CAD models into the existing combinatorial geometry format can be very difficult when it can be done, and may not be possible with some of the general surfaces employed within CAD.

There are disadvantages to this approach as well. Tolerances may be imposed throughout based on either the special generalized surfaces or perceived manufacturing precision. These can result in history rejection as the code can no longer continue to follow a trajectory. Many of these tolerances are already under user-control. For those that are not we hope to either engage the vendor or, as a last resort, modify the source code.

Another disadvantage is the run-time efficiency will not be as great as the existing combinatorial geometry approach. This is partly due to the mathematical representation, and partly due to the use of general commercial routines. We are willing to deliberately sacrifice some run-time for setup time as long as it is not excessive. Decreases in run-time efficiency arise from the following:

- In both the CG and CAD approaches, ray intersections with an object require ray intersections of the faces of that object. Typically each face is a part of a larger surface (e.g. sphere, infinite plane, etc.). Both models require calculation of ray intersections with these larger surfaces. Due to the explicit Boolean-algebra description used in CG, the object intersection follows immediately. However, in CAD additional calculations must be made for each surface intersection to determine if the ray truly intersects the object's face (i.e. the bounded part of the larger surface). This can be computationally expensive.
- In CG all space is defined, so ray intersections always involve leaving a single, well-defined region. In CAD, one typically describes objects and not the void or air between. Entering this region (the "ubiquitous void") can be determined as not being

anywhere else. Leaving this region also involves ray intersections with all other objects to be sure another object is not closer than the one presently being tested.

- The nature of CG involves Boolean descriptions of a library of specified primitives, so the same surfaces are often used on more than one object. In CAD, the objects tend to be described by their own set of faces (along with the bounds of those surfaces) which are often duplicated for adjacent objects.
- The generalized commercial routines may have spurious computations such as bulletin-board operations or dynamic memory allocation (which may be better done up-front in a pre-processing mode).

The CAD library routines can interrogate the geometry in the following manner:

1. Given a point and a direction, determine the closest boundary intersection.
2. Given a point, identify the region enclosing that point.
3. Given a point on a surface, determine the outgoing surface normal.
4. Given a point, determine the minimum distance to a boundary.

The fourth point above, only needed for range-rejection variance reduction, has not yet been implemented. We have replaced the second point with combinations of one and three, so that eventually the same ray intersections can be stored and retrieved to effectively answer the second question based on calculations already performed to answer the first.

We have created efficiency mechanisms in the code to address some of the run-time concerns listed above. These are based on avoiding unnecessary calculations, focusing a search, or performing simpler calculations:

- A regular grid is superposed on the entire geometry. Since it is regular, the grid itself requires no space and cell identification is trivial. A list is created of all regions that intersect each cell. Entering the "ubiquitous void" then only requires not being in all other regions within a cell.
- The CAD model includes a simple, bounding volume around each part and each face. If the ray misses the bounding volume, it surely will miss the object within.
- The code "learns" by remembering which regions can be entered while exiting a given region. Unfortunately, it is of no use to "learn" the "ubiquitous void" region can be entered.
- A "mailboxing" scheme was implemented in conjunction with the above learning logic. Once the code has exhausted the possible regions on the learning logic list without success, it will need to check all remaining zones to determine where it is headed. This scheme simply prevents checking the same zone more than once.
- A "screening" approach was implemented in conjunction with the above bounding-volume mechanism. Namely, even if a ray intersects the bounding volume of an object, that object only needs to be interrogated if the distance to enter that bounding volume is closer than the closest object already found.

Timing results for 10,000 histories in CAD geometry relative to CG are shown in Table 1. In all cases the use of screening on the CAD bounding volumes was activated and mailboxing was on when the learning logic was activated. The effectiveness of any

of the mechanisms is very problem dependent. These particular calculations were for adjoint charge deposition in a chip-sized volume in the STARSAT model.

Table 1 Efficiency of adjoint charge deposition in CAD geometry relative to CG.

Timing Ratio:	Grid	Learning
120	Off	Off
34	On	Off
27	On	On

For verification purposes, we have implemented a "mirroring" technique whereby CG and CAD can run at the same time for those cases where we have identical geometrical models. We have developed a simple translator that can create a CAD model from an existing CG representation for such purposes. In the "mirroring" mode, the CG code is running, but anytime a geometry query is made the CAD logic is also invoked and the two results are compared. The only time these disagree is when the CAD hits an unexpected tolerance that results in the rejection of that history. This only happens a small fraction of the time, and we are continuing to study the details of these situations.

6. CONCLUSIONS

A method for adjoint charge-deposition calculations has been developed and implemented in the multigroup ITS code. Numerical results have been compared with forward calculations and experimental data. These adjoint calculations were found to be computationally expensive, but in some cases this may be justified. Using the STARSAT geometry, the potential of this method was demonstrated for assessing charge-deposition vulnerabilities in complex, three-dimensional geometries. Methods used to transport particles in CAD-geometry models using the physics of ITS were discussed. Using CAD geometry yields less efficient Monte Carlo calculations but may save considerable amounts of time in preparing a CG model for the calculation.

NOMENCLATURE

N number of particles emerging from a particle interaction
Σ macroscopic cross section
E particle energy
ΔE_g energy width of group g
S stopping power
β CSD contribution of approximated group-to-group transfers
W weight of initiated adjoint particles

Subscripts

g arbitrary energy group
L lowest-energy group
t total inelastic Boltzmann-interaction cross section
a absorption cross section

c cutoff energy
dep charge-deposition cross section

Superscripts

m mid-point of energy group

ACKNOWLEDGMENTS

Sandia is a multiprogram laboratory operated by Sandia Corporation, a Lockheed Martin Company, for the United States Department of Energy under contract DE-AC04-94AL85000.

REFERENCES

Halbleib, J.A., Morel, J.E., 1980. Adjoint Monte Carlo electron transport in the continuous slowing-down approximation, *J. Comp. Phys.* **34**, 211.

Halbleib, J.A., Kensek, R.P., Valdez, G.D., Seltzer, S.M., Berger, M.J., 1992. ITS: the integrated TIGER series of electron/photon codes – version 3.0, *IEEE Trans. Nucl. Sci.* **39**, 1025.

Lockwood, G.J., Ruggles, L.E., Miller, G.H., Halbleib, J.A. Electron energy and charge albedos – calorimetric measurement vs Monte Carlo theory. Sandia National Laboratories SAND80-1968, November 1981.

Lorence Jr., L.J., Morel, J.E., Valdez, G.D. Physics guide to CEPXS: a multigroup coupled electron-photon cross-section generating code. Sandia National Laboratories SAND89-1685, October 1989.

Lorence, L.J., Kensek, R.P., Halbleib, J.A., Morel, J.E., 1995. Adjoint electron-photon transport Monte Carlo calculations with ITS. *IEEE Trans. Nucl. Sci.* **42**, 1895-1901.

Morel, J.E., Lorence, L.J., Kensek, R.P., Halbleib, J.A., Sloan, D.P., 1996. A hybrid multigroup/continuous-energy Monte Carlo method for solving the Boltzmann-Fokker-Planck equation. *Nucl. Sci. Eng.* **124**, 369-389.

Spatial Technology. ACIS 6.0 3D toolkit technical overview. Spatial Technology Inc., 2000.

Tabata, T., Rinsuke, I., Okabe, S., Fujita, Y., 1971. Charge distribution produced by 4- to 24-MeV electrons in elemental materials. *Phys. Rev. B* **3**, 572-583.

Varcolik, F.D., Adams, K.J., Tigner, J.E. STARSAT/Misty Rain radiation environment study. Volume 1 – model development. SAIC Report Number: SAIC-102-88-005, February 1988.